

Movable but unavoidable nodal lines through high-symmetry points in two-dimensional materials

V Damljanović

Institute of Physics Belgrade, University of Belgrade, Pregrevica 118, 11080 Belgrade, Serbia

E-mail: damlja@ipb.ac.rs

February 2023

Abstract. In two-dimensional materials electronic band contacts often give non-trivial contribution to materials topological properties. Besides band contacts at high-symmetry points (HSP) in the Brillouin zone (BZ), like those in graphene, there are nodal lines which form various patterns in the reciprocal space. In this paper we have found all movable nodal lines, which shape depends on the model, that pass through HSPs in the presence of time-reversal symmetry. Cases with and without spin-orbit coupling are included by studying all eighty layer groups and their double extensions. Eight single and six double groups, including three symmorphic, necessarily host Dirac and Weyl nodal lines that extend through the whole BZ, respectively. Our research might be of interest in designing new materials with interesting physical properties.

1. Introduction

Physics of two-dimensional (2D) materials became one of the focal points of solid-state science, since the electric field effect has been reported in atomically thin graphene in 2004. Brillouin zone (BZ) of 2D materials is an even-dimensional manifold, so topological invariants are used in explaining properties of 2D materials - such as integer quantum Hall effect. Non-zero topological charge originates from singularities of electron wave functions in the reciprocal space, and these singularities appear at BZ points where two or more electron bands touch [1].

In 2D, bands can touch at isolated points or lines. Band touchings can be essential [2, 3] or accidental [4]. The former are induced by the crystal and time-reversal symmetry (TRS), they are pinned to a high symmetry point (HSP) or line (HSL) and they are intact by symmetry preserving perturbations. Accidental band contacts change their position in the BZ by perturbations that keep the symmetry, they cannot be removed if protected by topology, or can be removed in the opposite case (truly accidental band contacts). So far, the existence of such movable but unavoidable nodal points (MNP) and lines (MNL) was almost exclusively linked to non-symmorphic symmetries of a crystal [5, 6, 7, 8, 9]. We show below that MNLs exist in some symmorphic groups too.

Nodal lines are further classified according to dispersion in the directions perpendicular to the line. For higher order nodal lines, the splitting is of order higher than one. In 3D non magnetic materials with spin-orbit coupling (SOC) such nodal lines are of order two and three [10]. Weyl (WNL) and Dirac nodal lines (DNL) have linear splitting, with two-fold and four-fold degeneracy on the line, respectively. Existence of WNL or DNL in bulk band structure leads to interesting physical properties, such as *drumhead* edge states, which are nearly dispersionless and hence exhibits strong electron correlations [11, 12]. Existence of nodal lines in 3D is connected with particular symmetry element [13, 14, 15, 16, 17, 18], and also analyzed by use of point groups [19], all 230 space groups [20] and with 3D magnetic groups [21]. These publications are augmented with exhaustive tables of all possible quasiparticles in 3D magnetic and non-magnetic crystals [22, 23, 24, 25, 26].

In 2D WNLs are predicted in GaTeI family [27] and in ferromagnetic layers [28, 29, 30]. For determination of properties of 2D materials using symmetry, characters or irreducible (co)representations of layer groups are necessary. Those are tabulated for layer double little groups [31], for generators of layer single groups [32] and for maximal symmetry of hexagonal materials [33]. Recently, full tabulation of layer groups, single and double, gray and ordinary is published [34]. We used [34] together with tables for (3D) space groups from Bilbao Crystallographic Server [35, 36] as a starting point of our research.

Here we present all MNLs that pass through HSPs in layer groups with TRS, with and without SOC. We show that these MNLs are unavoidable for crystals belonging to eight layer groups (describing systems without SOC), and six layer double groups (for crystals with SOC). We give dispersions and effective Hamiltonians near mentioned HSPs, and have illustrated our theory with few examples. An interesting curiosity are three symmorphic layer groups that support MNLs when SOC is included. Finally, we compare our results with those published in the literature on related topics.

2. Method

For \mathbf{k}_0 being a BZ point (HSP), \mathbf{q} a small wave vector, R allowed irreducible (co)representation of little group $G_{\mathbf{k}_0}$ of \mathbf{k}_0 and $g = \{\hat{h} | \tau_{\hat{h}}\}$ an element (in Seitz notation) of $G_{\mathbf{k}_0}$, the following formula holds [37]:

$$\widehat{H}(\mathbf{k}_0 + \mathbf{q}) = \widehat{R}^\dagger(g) \widehat{H}(\mathbf{k}_0 + \hat{h}'\mathbf{q}) \widehat{R}(g), \quad (1a)$$

where \hat{h}' is the operator reduction of \hat{h} to 2D BZ. If, in addition, $-\mathbf{k}_0$ belongs to the star of \mathbf{k}_0 , then TRS (denoted by θ) gives:

$$\widehat{H}'(\mathbf{q}) = \widehat{R}^\dagger(\theta g_s) \widehat{H}'(-\hat{h}'_s \mathbf{q}) \widehat{R}(\theta g_s), \quad (1b)$$

where $\widehat{H}'(\mathbf{q}) = \widehat{H}(\mathbf{k}_0 + \mathbf{q}) - \widehat{H}(\mathbf{k}_0)$, $g_s = \{\hat{h}_s | \tau_{\hat{h}_s}\}$ and $\hat{h}_s \mathbf{k}_0$ differs from $-\mathbf{k}_0$ by a reciprocal lattice vector. By differentiating these relations with respect to \mathbf{q} at $\mathbf{q} = 0$ once, twice,...*etc.* we get relations between Hamiltonian derivatives, and from there

we derive dispersions in the vicinity of HSP. We have considered Hamiltonians up to and including second (third) order for case without (with) SOC and we have isolated groups and HSPs that are not located at HSL and that have line-like solutions for vanishing splitting terms. In all such cases, two-component Hamiltonians contain only one Pauli matrix (in addition to the unit matrix) which we choose to be $\hat{\sigma}_1$. Since n -th order Hamiltonian derivatives transform as $[\Gamma_{2DPV}^{\otimes n}] \otimes R^* \otimes R$, and since in all cases of interest (except for double group 74^D -BZ center), $\Gamma_{2DPV}^{\otimes 3} = 4\Gamma_{2DPV}$ (or $\Gamma_{2DPV}^{\otimes 3} = 2\Gamma_1 + 3\Gamma_{2DPV}$, for 74^D -BZ center), we could exclude the possibility that some higher order derivatives couple to any other Pauli matrix, than the ones already contained in the linear or quadratic (linear, quadratic or cubic for 74^D -BZ center) terms in Hamiltonian Taylor expansion, which would cause energy splitting. Γ_{2DPV} denotes 2D polar-vector representation that acts in 2D reciprocal space, Γ_1 is the unit representation, while $[\Gamma_{2DPV}^{\otimes n}]$ is the symmetrised n -th power of Γ_{2DPV} . It turned out that four-component Hamiltonians, that do not correspond to fortune teller (FT) dispersion [38, 39], do not support MNLs. Since gray layer single and double groups have multidimensional little group correps of dimensions two and four, our method exhausts all possibilities.

We now prove that, if MNL exists in the vicinity of a HSP, it must continue further. For \mathbf{k}_0 now being touching point of two bands located near HSP, its little group contains only horizontal reflection plane as a nontrivial element. Both bands can be approximated with $E_1 = p_1q_1 + p_2q_2$ and $E_2 = c_1q_1 + c_2q_2$ respectively, so that $p_1 \neq c_1$ and $p_2 \neq c_2$ (at $\mathbf{q} = 0$ two bands touch by initial assumption, \mathbf{k}_0 is now not a HSP but lies close to it). Now $E_1 = E_2$ has solution $q_2 = q_1(p_1 - c_1)/(c_2 - p_2)$ which means that the line continues. We can repeat the same reasoning for the another point close to \mathbf{k}_0 and so on. In other words, MNL can not be interrupted.

Finally, guided by the result described in the previous paragraph, we have included groups that host FT states, described in [38] and [39] for non-SOC and SOC cases, respectively, and also experimentally observed [40]. Among conclusions of previous paragraph is that FT states cannot be the only features at the Fermi level. This holds no matter if Chern number of FT states is integer or not.

3. Results

In what follows, c 's denote real parameters, while q_1 and q_2 are projections of \mathbf{q} to orthonormal basis vectors \mathbf{e}_1 and \mathbf{e}_2 , respectively. The orientation of basis vectors is arbitrary since no little group of HSPs in question contains horizontal rotation axis or vertical reflection plane, except for groups hosting FT dispersion. However, depending on the parameters of the model, sometimes it is more convenient to switch to other orthonormal basis \mathbf{e}'_1 , \mathbf{e}'_2 , which will be defined below. In these cases projections of \mathbf{q} to this new basis are denoted with q'_1 and q'_2 . Finally $V_{l,m}^{(2)}$ ($V_{l,m,n}^{(3)}$) are second (third) order derivatives of certain components of the Hamiltonian. These are real parameters, symmetric under any permutation of indices, but with no additional symmetry. The

superscript D denotes double group, which is the symmetry of the system with SOC.

Groups and HSPs hosting MNL when SOC is neglected are shown in the Table 1, those with SOC in the Table 2. For groups 5, 7, 36, 48, 52 (points $(0, \pm 1/2)$, $(\pm 1/2, 0)$), 4^D , 5^D , 35^D and 74^D (points $(0, \pm 1/2)$, $(\pm 1/2, 0)$, $\pm(1/2, 1/2)$), the Hamiltonian and dispersion are:

$$\widehat{H} = \left(E_0 + \sum_{l,m=1}^2 V_{l,m}^{(2)} q_l q_m \right) \widehat{\sigma}_0 + \left(c_1 q_1 + c_2 q_2 + \sum_{l,m,n=1}^2 V_{l,m,n}^{(3)} q_l q_m q_n \right) \widehat{\sigma}_1, \quad (2a)$$

$$E_{1,2} = E_0 + \sum_{l,m=1}^2 V_{l,m}^{(2)} q_l q_m \pm |c_1 q_1 + c_2 q_2 + \sum_{l,m,n=1}^2 V_{l,m,n}^{(3)} q_l q_m q_n|. \quad (2b)$$

For new basis given by:

$$\mathbf{e}'_1 = \frac{c_1 \mathbf{e}_1 + c_2 \mathbf{e}_2}{\sqrt{c_1^2 + c_2^2}}, \quad (2c)$$

$$\mathbf{e}'_2 = \frac{-c_2 \mathbf{e}_1 + c_1 \mathbf{e}_2}{\sqrt{c_1^2 + c_2^2}},$$

the Hamiltonian and dispersion are:

$$\widehat{H} = \left(E_0 + \sum_{l,m=1}^2 V_{l,m}^{(2)} q'_l q'_m \right) \widehat{\sigma}_0 + \sqrt{c_1^2 + c_2^2} (q'_1 + c_0 q_2'^3) \widehat{\sigma}_1, \quad (2d)$$

$$E_{1,2} = E_0 + \sum_{l,m=1}^2 V_{l,m}^{(2)} q'_l q'_m \pm \sqrt{c_1^2 + c_2^2} |q'_1 + c_0 q_2'^3|, \quad (2e)$$

with $c_0 = (c_1^3 V_{222}^{(3)} - 3c_1^2 c_2 V_{122}^{(3)} + 3c_1 c_2^2 V_{112}^{(3)} - c_2^3 V_{111}^{(3)}) / (c_1^2 + c_2^2)^2$. Since $q'_1 + c_0 q_2'^3 = 0$ has one solution, one MNL passes through $\mathbf{q} = 0$. In (2d) and (2e) we have neglected energy splitting terms that contain products of q'_1 with q_2' , in comparison to q_1' . Such HSPs were mentioned in [41] as having linearity rank one.

For group 52 near BZ corners, the following relations hold:

$$\widehat{H} = (E_0 + c\mathbf{q}^2) \widehat{\sigma}_0 + (c_1 q_1^2 + c_2 q_1 q_2 - c_1 q_2^2) \widehat{\sigma}_1, \quad (3a)$$

$$E_{1,2} = E_0 + c\mathbf{q}^2 \pm |c_1 q_1^2 + c_2 q_1 q_2 - c_1 q_2^2|. \quad (3b)$$

In the new basis:

$$\mathbf{e}'_1 = \frac{\mathbf{e}_1 + \lambda \mathbf{e}_2}{\sqrt{1 + \lambda^2}}, \quad (3c)$$

$$\mathbf{e}'_2 = \frac{-\lambda \mathbf{e}_1 + \mathbf{e}_2}{\sqrt{1 + \lambda^2}},$$

where $\lambda = (c_2 + \sqrt{c_2^2 + 4c_1^2}) / (2c_1)$, the following holds:

$$\widehat{H} = (E_0 + c\mathbf{q}'^2) \widehat{\sigma}_0 - \sqrt{c_2^2 + 4c_1^2} q'_1 q_2' \widehat{\sigma}_1, \quad (3d)$$

Table 1. Layer single groups hosting unavoidable accidental nodal lines through HSP. The notation for layer and space groups as well as primitive basis vectors are according to [42] and [43], respectively. The coordinates of HSPs in the last column, are in the primitive basis $\{\mathbf{b}_1, \mathbf{b}_2\}$ of the reciprocal 2D lattice.

Layer single group	Corresponding space group	Diperiodic plane	HSP
5 $p 1 1 b$	7 $P 1 c 1$	C_s^2	$y = 0$ $(0, \pm\frac{1}{2})$ $(\pm\frac{1}{2}, \pm\frac{1}{2})$
7 $p 1 1 2/b$	13 $P 1 2/c 1$	C_{2h}^4	$y = 0$ $(0, \pm\frac{1}{2})$ $(\pm\frac{1}{2}, \pm\frac{1}{2})$
33 $p b 2_1 a$	29 $P c a 2_1$	C_{2v}^5	$y = 0$ $(\pm\frac{1}{2}, \pm\frac{1}{2})$
36 $c m 2 e$	39 $A e m 2$	C_{2v}^{15}	$x = 0$ $(0, \pm\frac{1}{2})$ $(\pm\frac{1}{2}, 0)$
43 $p 2/b 2_1/a 2/a$	54 $P 2_1/c 2/c 2/a$	D_{2h}^8	$y = 0$ $(\pm\frac{1}{2}, \pm\frac{1}{2})$
45 $p 2_1/b 2_1/m 2/a$	57 $P 2/b 2_1/c 2_1/m$	D_{2h}^{11}	$x = 0$ $(\pm\frac{1}{2}, \pm\frac{1}{2})$
48 $c 2/m 2/m 2/e$	67 $C 2/m 2/m 2/e$	D_{2h}^{21}	$z = 0$ $(0, \pm\frac{1}{2})$ $(\pm\frac{1}{2}, 0)$
52 $p 4/n$	85 $P 4/n$	C_{4h}^3	$z = 0$ $(0, \pm\frac{1}{2})$ $(\pm\frac{1}{2}, 0)$ $(\pm\frac{1}{2}, \pm\frac{1}{2})$

Table 2. Layer double groups hosting unavoidable accidental nodal lines through HSP. The notation for layer and space groups as well as primitive basis vectors are according to [42] and [43], respectively. The coordinates of HSPs in the last column, are in the primitive basis $\{\mathbf{b}_1, \mathbf{b}_2\}$ of the reciprocal 2D lattice.

Layer double group	Corresponding space double group	Diperiodic plane	HSP
4^D $p 1 1 m$	6^D $P 1 m 1$	C_s^1	$y = 0$ $(0, 0)$ $(\pm\frac{1}{2}, 0)$ $(0, \pm\frac{1}{2})$ $(\pm\frac{1}{2}, \pm\frac{1}{2})$
5^D $p 1 1 b$	7^D $P 1 c 1$	C_s^2	$y = 0$ $(0, 0)$ $(\pm\frac{1}{2}, 0)$
29^D $p b 2_1 m$	26^D $P m c 2_1$	C_{2v}^2	$x = 0$ $(0, \pm\frac{1}{2})$ $(\pm\frac{1}{2}, \pm\frac{1}{2})$
33^D $p b 2_1 a$	29^D $P c a 2_1$	C_{2v}^5	$y = 0$ $(0, \pm\frac{1}{2})$
35^D $c m 2 m$	38^D $A m m 2$	C_{2v}^{14}	$x = 0$ $(0, \pm\frac{1}{2})$ $(\pm\frac{1}{2}, 0)$
74^D $p \bar{6}$	174^D $P \bar{6}$	C_{3h}^1	$z = 0$ $(0, 0)$ $(\pm\frac{1}{2}, 0)$ $(0, \pm\frac{1}{2})$ $\pm(\frac{1}{2}, \frac{1}{2})$

$$E_{1,2} = E_0 + c\mathbf{q}^{\prime 2} \pm \sqrt{c_2^2 + 4c_1^2|q_1'q_2'|}. \quad (3e)$$

Since $q_1'q_2' = 0$ has two solutions, two MNL intersect at right angle for $\mathbf{q} = 0$.

For group 74^D near the BZ center ($\mathbf{k}_0 = 0$):

$$\widehat{H} = (E_0 + c\mathbf{q}^2) \widehat{\sigma}_0 + (c_1q_1(q_1^2 - 3q_2^2) + c_2q_2(q_2^2 - 3q_1^2)) \widehat{\sigma}_1, \quad (4a)$$

$$E_{1,2} = E_0 + c\mathbf{q}^2 \pm |c_1q_1(q_1^2 - 3q_2^2) + c_2q_2(q_2^2 - 3q_1^2)|. \quad (4b)$$

New basis is given by:

$$\mathbf{e}'_1 = \frac{c_2\mathbf{e}_1 + c_1B\mathbf{e}_2}{\sqrt{c_2^2 + c_1^2B^2}}, \quad (4c)$$

$$\mathbf{e}'_2 = \frac{-c_1B\mathbf{e}_1 + c_2\mathbf{e}_2}{\sqrt{c_2^2 + c_1^2B^2}},$$

where $B = 1 + 2\sqrt{1 + c_2^2/c_1^2} \cos[(1/3)\arccos(1/\sqrt{1 + c_2^2/c_1^2})]$ is a real solution of the cubic equation $(c_1/c_2)^2B^3 - 3(c_1/c_2)^2B^2 - 3B + 1 = 0$. In the new basis the Hamiltonian and dispersion are:

$$\widehat{H} = (E_0 + c\mathbf{q}^{\prime 2}) \widehat{\sigma}_0 - \frac{c_1^2(B^2 - 2B) - c_2^2}{\sqrt{c_2^2 + c_1^2B^2}} q_2'(q_2^{\prime 2} - 3q_1^{\prime 2}) \widehat{\sigma}_1, \quad (4d)$$

$$E_{1,2} = E_0 + c\mathbf{q}^{\prime 2} \pm \frac{c_1^2(B^2 - 2B) - c_2^2}{\sqrt{c_2^2 + c_1^2B^2}} |q_2'(q_2^{\prime 2} - 3q_1^{\prime 2})|. \quad (4e)$$

Here we note that $c_1^2(B^2 - 2B) - c_2^2 > 0$. Since $q_2'(q_2^{\prime 2} - 3q_1^{\prime 2}) = 0$ has three solutions, three MNL intersects at $\mathbf{q} = 0$ at angles of $\pi/3$.

Groups 33, 43, 45, 29^D and 33^D host fortune teller (FT) dispersion which is described in more detail in [38, 39]. Here we only give the dispersion:

$$E_{j,l} = j|c_1|q_1| + l|c_2|q_2|, (j, l \in \{+, -\}), \quad (5)$$

where c_1 and c_2 are (only in this formula) positive quantities. Bands are ordered in the following way: $E_{-,+} \leq E_{-,-} \leq E_{+,-} \leq E_{+,+}$. It follows that MNLs $E_{-,-} = E_{+,-}$ are given by $c_1q_1 = c_2q_2$ and $c_1q_1 = -c_2q_2$. Two MNLs intersect at $\mathbf{q} = 0$ at an angle that is dependent on c_1 and c_2 . Those MNLs arising from FT dispersion are at constant energy only in linear approximation. When quadratic corrections to the Hamiltonian are accounted for, the MNL remain unsplit but overall energy shift is quadratic in q_{\parallel} - the wave vector along MNL.

4. Illustrative examples

We first consider the tight-binding model from the s -orbitals, without SOC, on the structure shown in Figure 1a), that belongs to layer group $p112/b$ (7). Occupied Wyckoff

position is $2d$ with $z = 1.3\text{\AA}$. The Hamiltonian and its eigenvalues are:

$$\widehat{H}(\mathbf{k}) = \begin{pmatrix} f_0 + 2f_1 \cos(\mathbf{k} \cdot \mathbf{a}_1) & 2e^{-\frac{i}{2}\mathbf{k} \cdot \mathbf{a}_2} (f_2 \cos(\frac{1}{2}\mathbf{k} \cdot \mathbf{a}_2) + f_3 \cos(\mathbf{k} \cdot \mathbf{a}_1 - \frac{1}{2}\mathbf{k} \cdot \mathbf{a}_2)) \\ 2e^{\frac{i}{2}\mathbf{k} \cdot \mathbf{a}_2} (f_2 \cos(\frac{1}{2}\mathbf{k} \cdot \mathbf{a}_2) + f_3 \cos(\mathbf{k} \cdot \mathbf{a}_1 - \frac{1}{2}\mathbf{k} \cdot \mathbf{a}_2)) & f_0 + 2f_1 \cos(\mathbf{k} \cdot \mathbf{a}_1) \end{pmatrix}, \quad (6a)$$

$$E_{1,2}(\mathbf{k}) = f_0 + 2f_1 \cos(\mathbf{k} \cdot \mathbf{a}_1) \pm 2|f_2 \cos(\frac{1}{2}\mathbf{k} \cdot \mathbf{a}_2) + f_3 \cos(\mathbf{k} \cdot \mathbf{a}_1 - \frac{1}{2}\mathbf{k} \cdot \mathbf{a}_2)|. \quad (6b)$$

Here f_0 , f_1 , f_2 and f_3 are hopping real parameters for zeroth, first, second and third neighbors, respectively. The two energies coincide for:

$$\mathbf{k} \cdot \mathbf{a}_2 \in \left\{ -2\arctan\left(\frac{f_2 + f_3 \cos(\mathbf{k} \cdot \mathbf{a}_1)}{f_3 \sin(\mathbf{k} \cdot \mathbf{a}_1)}\right) + 2m\pi \right\}, \quad (6c)$$

where m is any integer. Equation (6c) is well defined for all possible values of hopping parameters. The full band structure for particular values of parameters is shown in Figure 1b), where band touching lines are clearly visible. Position of lines in the reciprocal space are shown in Figure 1c). By varying parameters, the shape of lines changes but the lines always pass through points $(0, 1/2)$ and $(1/2, 1/2)$ and equivalent to them, as shown in Table 1 and Figure 1c), d).

We next consider the tight-binding model on the structure shown in Figure 2a) that belongs to symmorphic layer (double) group $p11m$ (4^D). We choose basis functions $|s_1 \uparrow\rangle, |s_1 \downarrow\rangle, |s_2 \uparrow\rangle, |s_2 \downarrow\rangle$, where s_1, s_2 are s -orbitals for atoms 1 and 2, respectively, while \uparrow and \downarrow denote spinors for up and down spin, respectively. Since horizontal reflection plane is symmetry of the system, the *up* and *down* states are decoupled from each other, so that Hamiltonian is block-diagonal:

$$\widehat{H} = \begin{pmatrix} \widehat{H}_\uparrow & \widehat{0} \\ \widehat{0} & \widehat{H}_\downarrow \end{pmatrix}, \quad (7a)$$

with

$$\widehat{H}_\uparrow(\mathbf{k}) = \widehat{H}_\downarrow^*(-\mathbf{k}) = \begin{pmatrix} f_0 & z_1 e^{-i\mathbf{k} \cdot \mathbf{a}_1} + z_2 + z_3 e^{i\mathbf{k} \cdot (\mathbf{a}_2 - \mathbf{a}_1)} \\ z_1^* e^{i\mathbf{k} \cdot \mathbf{a}_1} + z_2^* + z_3^* e^{-i\mathbf{k} \cdot (\mathbf{a}_2 - \mathbf{a}_1)} & g_0 \end{pmatrix}. \quad (7b)$$

Here f_0 and g_0 are real, on-site hopping parameters for sites 1 and 2, respectively, while z_1 , z_2 and z_3 are complex hopping parameters for first, second and third neighbors, respectively. The full band structure is:

$$E_2^{\uparrow, \downarrow}(\mathbf{k}) = \frac{f_0 + g_0}{2} + \frac{1}{2} \sqrt{(f_0 - g_0)^2 + 4|z_1 e^{\mp i\mathbf{k} \cdot \mathbf{a}_1} + z_2 + z_3 e^{\pm i\mathbf{k} \cdot (\mathbf{a}_2 - \mathbf{a}_1)}|^2}, \quad (7c)$$

$$E_1^{\uparrow, \downarrow}(\mathbf{k}) = \frac{f_0 + g_0}{2} - \frac{1}{2} \sqrt{(f_0 - g_0)^2 + 4|z_1 e^{\mp i\mathbf{k} \cdot \mathbf{a}_1} + z_2 + z_3 e^{\pm i\mathbf{k} \cdot (\mathbf{a}_2 - \mathbf{a}_1)}|^2}. \quad (7d)$$

Both nodal lines $E_1^\uparrow = E_1^\downarrow$ and $E_2^\uparrow = E_2^\downarrow$ are given by the equation:

$$h_3 \sin(\mathbf{k} \cdot \mathbf{a}_1) + h_2 \sin(\mathbf{k} \cdot \mathbf{a}_2) + h_1 \sin[\mathbf{k} \cdot (\mathbf{a}_2 - \mathbf{a}_1)] = 0, \quad (7e)$$

where $h_1 = -i(z_2^* z_3 - z_2 z_3^*)$, $h_2 = -i(z_1^* z_3 - z_1 z_3^*)$ and $h_3 = -i(z_1^* z_2 - z_1 z_2^*)$ are real parameters. Equation (7e) has the following solution:

$$\mathbf{k} \cdot \mathbf{a}_2 \in \left\{ \Phi - \arcsin\left(\frac{h_3}{h_1} \sin\Phi\right) + 2m\pi, \Phi + \arcsin\left(\frac{h_3}{h_1} \sin\Phi\right) + (2m+1)\pi \right\}, \quad (7f)$$

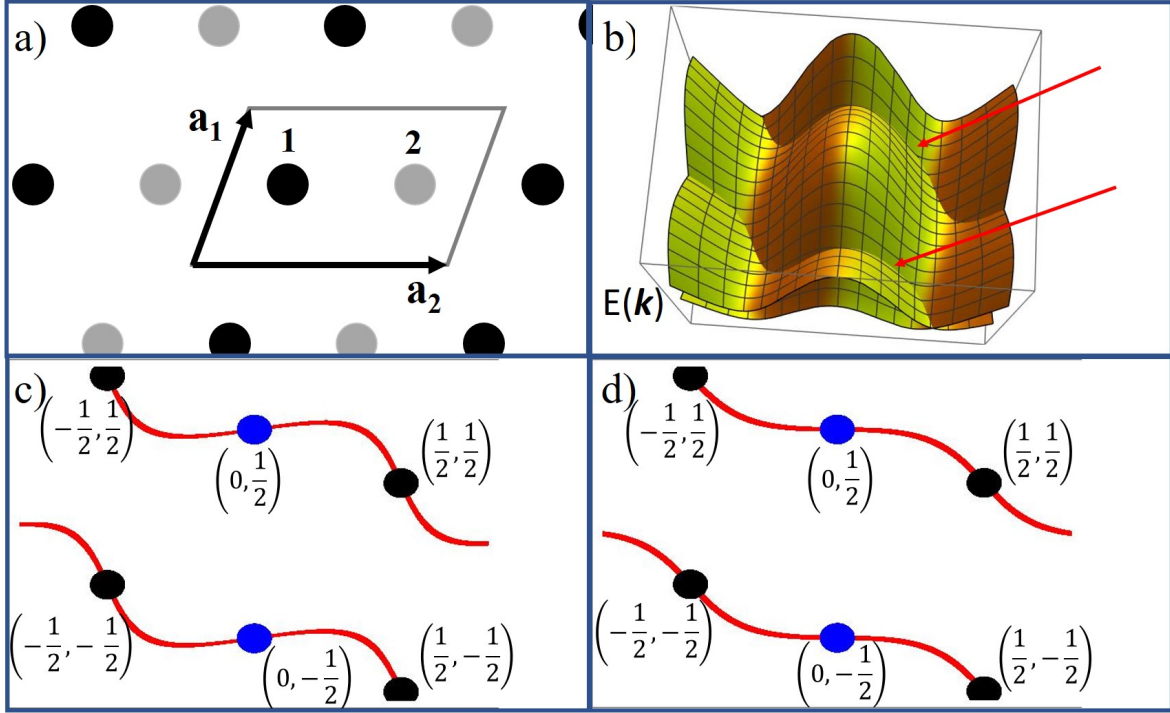


Figure 1. Tight binding model for $p112/b$: a) - crystal structure (all nuclei are of the same type, black and gray circles denotes nuclei above and below the drawing plane, respectively, visualization by VESTA [44]), b) - electronic band structure for f_0, f_1, f_2 and f_3 equal to 4.2, 1.3, 0.9 and 0.5 in arbitrary units (*a.u.*), respectively (red arrows denote MNLs), c) - position of MNL in the reciprocal space, d) - same as c) for f_0, f_1, f_2 and f_3 equal to 3.6, 3.1, 2.7 and 0.9 *a.u.*, respectively. In c) and d) numbers in brackets denote coordinates of special points in the reciprocal basis (blue and black circles). Mutually equivalent points are denoted with circles of the same color.

with m being any integer and

$$\sin(\Phi) = \frac{h_1 \sin(\mathbf{k} \cdot \mathbf{a}_1) / h_3}{\sqrt{(h_1^2 + h_2^2) / h_3^2 + 2h_1 h_2 \cos(\mathbf{k} \cdot \mathbf{a}_1) / h_3^2}}, \quad (7g)$$

$$\cos(\Phi) = \frac{h_1 \cos(\mathbf{k} \cdot \mathbf{a}_1) / h_3 + h_2 / h_3}{\sqrt{(h_1^2 + h_2^2) / h_3^2 + 2h_1 h_2 \cos(\mathbf{k} \cdot \mathbf{a}_1) / h_3^2}}. \quad (7h)$$

The argument of \arcsin in (7f) has modulus less or equal to one except if $(h_1/h_3)^2$ and $(h_2/h_3)^2$ are both less than one. In that case $-1 \leq \cos(\mathbf{k} \cdot \mathbf{a}_1) \leq t_2$ or $t_1 \leq \cos(\mathbf{k} \cdot \mathbf{a}_1) \leq 1$ must hold ($t_{1,2} = -h_1 h_2 / h_3^2 \pm \sqrt{(1 - h_1^2 / h_3^2)(1 - h_2^2 / h_3^2)}$). Band structure shown in Figure 2b) for particular values of parameters, confirm existence of MNL. In this case h_1^2 and h_2^2 are both less than h_3^2 , while in the case shown in Figure 2d) this does not hold, with the clear difference in accidental degeneracy pattern. In any case, MNLs pass through HSPs as shown in Table 2 and in Figure 2c), d).

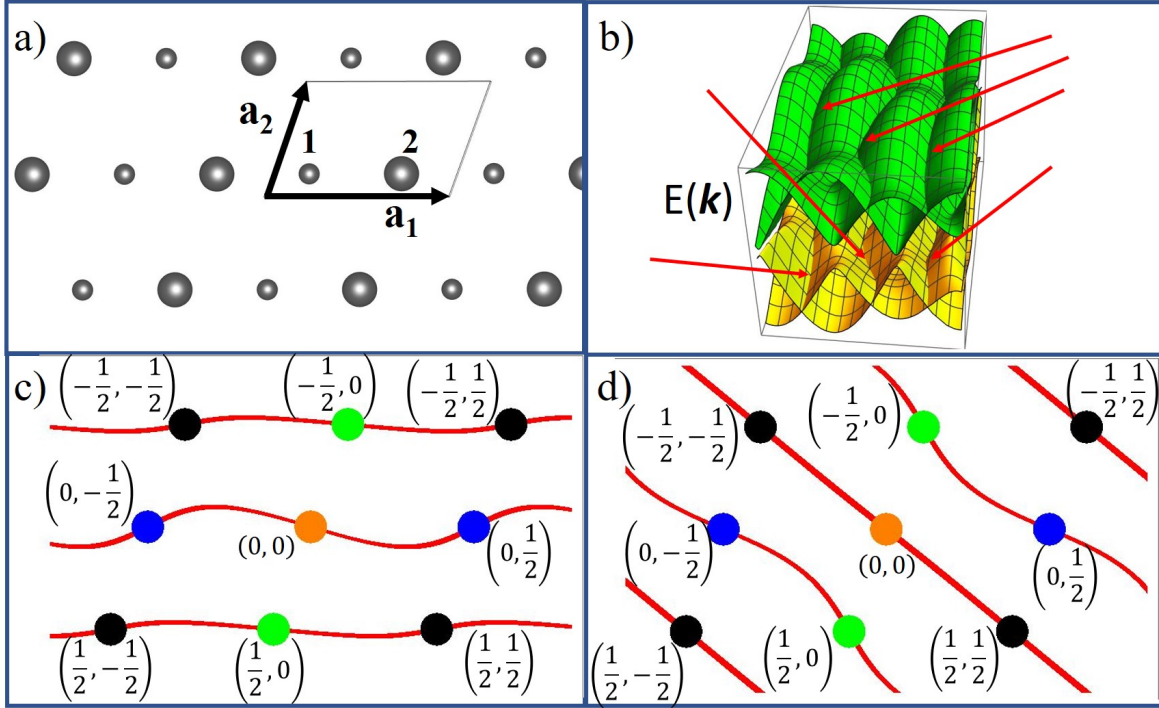


Figure 2. Tight binding model for symmorphic $p11m$: a) - crystal structure (nuclei of both types are located at one plane, visualization by VESTA [44]), b) - electronic band structure for f_0, f_1, z_1, z_2 and z_3 equal to 2, 3, $4 + 2i$, $3 - 6i$ and $1 + 2i$ *a.u.*, respectively (red arrows denote MNLs), c) - position of MNL in the reciprocal space, d) - same as c) for f_0, f_1, z_1, z_2 and z_3 equal to 4.2, 1.3, $-2.4 + 1.2i$, $3.4 - 5.6i$ and $6.1 + 1.2i$ *a.u.*, respectively. In c) and d) numbers in brackets denote coordinates of special points in the reciprocal basis (blue, orange, green and black circles). Mutually equivalent points are denoted with circles of the same color.

5. Discussion and conclusions

We compare our results with the ones on related topics published in the literature. Analysis of all 3D crystallographic point double groups, for systems with SOC, that shows in which cases movable or unmovable nodal lines exist is reported [45]. Their results can be used for symmorphic little groups, since then allowed representations are just a product of point group irreducible representations with the phase factors that represent translations. Point groups \underline{C}_s^D and \underline{C}_{3h}^D hosts one and three MNL, respectively [45]. This is in accordance with our results in Table 2 (little group for 74^D in BZ center is \underline{C}_{3h}^D , for remaining symmorphic groups it is \underline{C}_s^D). On the other hand, HSPs for non-symmorphic 29^D and 33^D from Table 2 host two intersecting MNL, while [45] predicts one nodal line along axis of order 2 for \underline{C}_{2v}^D . This difference is because 29^D and 33^D are non-symmorphic and because band degeneracy at HSPs hosting FT states is four, while [45] considers two-band models.

Origin of doubly degenerate nodal lines that connect time-reversal invariant momenta in 3D crystals with SOC is reported in [46]. List of symmorphic 3D space

groups that host such lines [46] contains all symmorphic corresponding space groups in Table 2, which support our findings. Compound PbTaSe_2 is a symmorphic 3D metal with SOC that exhibits nodal lines in experiments [47], as predicted in [46]. To avoid Kramers degeneracy in the whole BZ, authors of [46] considered non-centrosymmetric 3D crystals. They show that nodal line through HSP exists if its little groups have at least one improper rotation (symmetry element with determinant -1). In our cases this is always fulfilled, since at least horizontal plane must be present in order to avoid band repulsion due to non-crossing rule.

To illustrate their own results, authors of [48] used tight binding model with SOC on a structure that belongs to group 74^D ($p\bar{6}$). Three nodal lines intersects symmetrically at BZ-center and also pass through middle of BZ edges, thus confirming our prediction. Numerical calculations [49] suggest that boron bilayer adopts structure with the symmetry $p\bar{6}$. Since boron is light element, reported band structure is without SOC [49]. Future research could show if it is possible to enhance SOC using bilayer boron as a starting material.

Group theoretical conditions for semi-Dirac dispersion in non-magnetic 2D materials with negligible SOC are reported [50]. All groups and HSPs from [50] are here included in Table 1. Tight-binding model for group $c 2/m 2/m 2/e$ gives line of degeneracy which depends on numerical values of tight-binding parameters [50], hence it is a MNL as predicted here. Moreover, the dispersion near $(0, 1/2)$ point in [50], matches the one for group $c 2/m 2/m 2/e$ given here in (2e). Similarly, tight-binding model for group $p 1 1 b$ published in [51], exhibits MNL across the whole BZ with the same dispersion near HSPs indicated in Table 1. Lines of accidental degeneracy, noticed in [51], gained full explanation in the present work. Group $c m 2 e$ is omitted in [50], due to a bug in REPRES program on Bilbao Crystallographic Server, which is fixed recently. According to [50], authors used REPRES [35] for finding allowed representations of layer groups via their corresponding space groups. Finally, one can point out that groups from [50] give semi-Dirac dispersion (quadratic in one direction of the BZ that split linearly in the perpendicular direction) while the bands do not form cones. Formation of semi-Dirac cones requires Hamiltonian of the form: $c_1 q_1 \hat{\sigma}_j + c_2 q_2^2 \hat{\sigma}_l$ (or, in more general case: $c_1 q_1 \hat{\sigma}_j + c_2 q_2^n \hat{\sigma}_l$), with two different Pauli matrices ($j \neq l$) and with n -natural number greater than one. We have omitted term with the unit matrix $\hat{\sigma}_0$, since it does not lead to band splitting. In this case the band splitting is: $\pm \sqrt{c_1^2 q_1^2 + c_2^2 q_2^4}$ (in more general case: $\pm \sqrt{c_1^2 q_1^2 + c_2^2 q_2^{2n}}$), with $\mathbf{q} = 0$ as the only touching point. Detail analysis of all HSP of all gray layer single or double groups does not give any HSP with semi-Dirac cones [41].

In summary we have determined all layer groups that host nodal lines through high-symmetry BZ points, which shape depends on the model parameters (MNL). In our analysis we have included both cases without and with SOC in the presence of TRS. Although we didn't restrict our search to Weyl or Dirac nodal lines only, it turned out that all MNL we found are either DNL (in cases without SOC) or WNL (in cases with SOC). Since little group representations responsible for MNLs are the only allowed in

listed HSPs, the existence of MNLs is guaranteed by the layer groups from Tables 1 and 2. On the other hand, it is not guaranteed that MNLs are at constant energy, nor that they lie close to the Fermi level, although such cases are not necessarily excluded. Our finding extend the knowledge of band degeneracies in 2D materials and might be useful for designing 2D materials which sensitivity to external conditions like temperature, pressure, strain *etc* is yet to be studied.

Acknowledgments

Author acknowledge funding by the Ministry of Science, Technological Development and Innovation of the Republic of Serbia provided by the Institute of Physics Belgrade, University of Belgrade.

References

- [1] Xiaolong Feng, Jiaojiao Zhu, Weikang Wu, and Shengyuan A. Yang. Two-dimensional topological semimetals. *Chinese Physics B*, 30(10):107304, nov 2021.
- [2] L. P. Bouckaert, R. Smoluchowski, and E. Wigner. Theory of Brillouin zones and symmetry properties of wave functions in crystals. *Phys. Rev.*, 50:58–67, Jul 1936.
- [3] Conyers Herring. Effect of time-reversal symmetry on energy bands of crystals. *Phys. Rev.*, 52:361–365, Aug 1937.
- [4] Conyers Herring. Accidental degeneracy in the energy bands of crystals. *Phys. Rev.*, 52:365–373, Aug 1937.
- [5] Steve M. Young and Charles L. Kane. Dirac semimetals in two dimensions. *Phys. Rev. Lett.*, 115:126803, Sep 2015.
- [6] Benjamin J. Wieder and C. L. Kane. Spin-orbit semimetals in the layer groups. *Phys. Rev. B*, 94:155108, Oct 2016.
- [7] J. Zhang, Y.-H. Chan, C.-K. Chiu, M. G. Vergniory, L. M. Schoop, and A. P. Schnyder. Topological band crossings in hexagonal materials. *Phys. Rev. Materials*, 2:074201, Jul 2018.
- [8] Moritz M. Hirschmann, Andreas Leonhardt, Berkay Kilic, Douglas H. Fabini, and Andreas P. Schnyder. Symmetry-enforced band crossings in tetragonal materials: Dirac and Weyl degeneracies on points, lines, and planes. *Phys. Rev. Materials*, 5:054202, May 2021.
- [9] Andreas Leonhardt, Moritz M. Hirschmann, Niclas Heinsdorf, Xianxin Wu, Douglas H. Fabini, and Andreas P. Schnyder. Symmetry-enforced topological band crossings in orthorhombic crystals: Classification and materials discovery. *Phys. Rev. Materials*, 5:124202, Dec 2021.
- [10] Zhi-Ming Yu, Weikang Wu, Xian-Lei Sheng, Y. X. Zhao, and Shengyuan A. Yang. Quadratic and cubic nodal lines stabilized by crystalline symmetry. *Phys. Rev. B*, 99:121106, Mar 2019.
- [11] Chen Fang, Hongming Weng, Xi Dai, and Zhong Fang. Topological nodal line semimetals. *Chinese Physics B*, 25(11):117106, nov 2016.
- [12] Shuo-Ying Yang, Hao Yang, Elena Derunova, Stuart S. P. Parkin, Binghai Yan, and Mazhar N. Ali. Symmetry demanded topological nodal-line materials. *Advances in Physics: X*, 3(1):1414631, 2018.
- [13] Chen Fang, Yige Chen, Hae-Young Kee, and Liang Fu. Topological nodal line semimetals with and without spin-orbital coupling. *Phys. Rev. B*, 92:081201, Aug 2015.
- [14] Youngkuk Kim, Benjamin J. Wieder, C. L. Kane, and Andrew M. Rappe. Dirac line nodes in inversion-symmetric crystals. *Phys. Rev. Lett.*, 115:036806, Jul 2015.
- [15] Zihao Gao, Meng Hua, Haijun Zhang, and Xiao Zhang. Classification of stable Dirac and Weyl semimetals with reflection and rotational symmetry. *Phys. Rev. B*, 93:205109, May 2016.

- [16] Bohm-Jung Yang, Troels Arnfred Bojesen, Takahiro Morimoto, and Akira Furusaki. Topological semimetals protected by off-centered symmetries in nonsymmorphic crystals. *Phys. Rev. B*, 95:075135, Feb 2017.
- [17] Zhida Song, Tiantian Zhang, and Chen Fang. Diagnosis for nonmagnetic topological semimetals in the absence of spin-orbital coupling. *Phys. Rev. X*, 8:031069, Sep 2018.
- [18] Heqiu Li, Chen Fang, and Kai Sun. Diagnosis of topological nodal lines with nontrivial monopole charge in the presence of rotation symmetries. *Phys. Rev. B*, 100:195308, Nov 2019.
- [19] Shingo Kobayashi, Youichi Yamakawa, Ai Yamakage, Takumi Inohara, Yoshihiko Okamoto, and Yukio Tanaka. Crossing-line-node semimetals: General theory and application to rare-earth trihydrides. *Phys. Rev. B*, 95:245208, Jun 2017.
- [20] Lin Wu, Feng Tang, and Xiangang Wan. Symmetry-enforced band nodes in 230 space groups. *Phys. Rev. B*, 104:045107, Jul 2021.
- [21] Jian Yang, Chen Fang, and Zheng-Xin Liu. Symmetry-protected nodal points and nodal lines in magnetic materials. *Phys. Rev. B*, 103:245141, Jun 2021.
- [22] Feng Tang and Xiangang Wan. Exhaustive construction of effective models in 1651 magnetic space groups. *Phys. Rev. B*, 104:085137, Aug 2021.
- [23] Zhi-Ming Yu, Zeying Zhang, Gui-Bin Liu, Weikang Wu, Xiao-Ping Li, Run-Wu Zhang, Shengyuan A. Yang, and Yugui Yao. Encyclopedia of emergent particles in three-dimensional crystals. *Science Bulletin*, 67(4):375–380, 2022.
- [24] Gui-Bin Liu, Zeying Zhang, Zhi-Ming Yu, Shengyuan A. Yang, and Yugui Yao. Systematic investigation of emergent particles in type-III magnetic space groups. *Phys. Rev. B*, 105:085117, Feb 2022.
- [25] Zeying Zhang, Gui-Bin Liu, Zhi-Ming Yu, Shengyuan A. Yang, and Yugui Yao. Encyclopedia of emergent particles in type-IV magnetic space groups. *Phys. Rev. B*, 105:104426, Mar 2022.
- [26] Feng Tang and Xiangang Wan. Complete classification of band nodal structures and massless excitations. *Phys. Rev. B*, 105:155156, Apr 2022.
- [27] Weikang Wu, Yalong Jiao, Si Li, Xian-Lei Sheng, Zhi-Ming Yu, and Shengyuan A. Yang. Hourglass Weyl loops in two dimensions: Theory and material realization in monolayer GaTeI family. *Phys. Rev. Mater.*, 3:054203, May 2019.
- [28] Baojie Feng, Run-Wu Zhang, Ya Feng, Botao Fu, Shilong Wu, Koji Miyamoto, Shaolong He, Lan Chen, Kehui Wu, Kenya Shimada, Taichi Okuda, and Yugui Yao. Discovery of Weyl nodal lines in a single-layer ferromagnet. *Phys. Rev. Lett.*, 123:116401, Sep 2019.
- [29] Lei Jin, Xiaoming Zhang, Tingli He, Weizhen Meng, Xuefang Dai, and Guodong Liu. Ferromagnetic two-dimensional metal-chlorides MCl ($M = Sc, Y$, and La): Candidates for Weyl nodal line semimetals with small spin-orbit coupling gaps. *Applied Surface Science*, 520:146376, 2020.
- [30] Feng Zhou, Ying Liu, Minquan Kuang, Peng Wang, Jianhua Wang, Tie Yang, Xiaotian Wang, Zhenxiang Cheng, and Gang Zhang. Time-reversal-breaking Weyl nodal lines in two-dimensional A_3C_2 ($A = Ti, Zr$, and Hf) intrinsically ferromagnetic materials with high Curie temperature. *Nanoscale*, 13:8235–8241, 2021.
- [31] D. B. Litvin and T. R. Wike. *Character Tables and Compatibility Relations of the Eighty Layer Groups and Seventeen Plane Groups*. Plenum Press, 1991.
- [32] I Milosevic, B Nikolic, M Damnjanovic, and M Krmar. Irreducible representations of diperiodic groups. *Journal of Physics A: Mathematical and General*, 31(15):3625, apr 1998.
- [33] V Damljanić, R Kostić, and R Gajić. Characters of graphene’s symmetry group $Dg80$. *Physica Scripta*, 2014(T162):014022, sep 2014.
- [34] Božidar Nikolić, Ivanka Milošević, Tatjana Vuković, Nataša Lazić, Saša Dmitrović, Zoran Popović, and Milan Damnjanović. Irreducible and site-symmetry-induced representations of single/double ordinary/grey layer groups. *Acta Crystallographica Section A*, 78(2):107–114, Mar 2022.
- [35] Mois I. Aroyo, Asen Kirov, Cesar Capillas, J. M. Perez-Mato, and Hans Wondratschek. Bilbao

- Crystallographic Server. II. Representations of crystallographic point groups and space groups. *Acta Crystallographica Section A*, 62(2):115–128, Mar 2006.
- [36] Luis Elcoro, Barry Bradlyn, Zhijun Wang, Maia G. Vergniory, Jennifer Cano, Claudia Felser, B. Andrei Bernevig, Danel Orobengoa, Gemma de la Flor, and Mois I. Aroyo. Double crystallographic groups and their representations on the Bilbao Crystallographic Server. *Journal of Applied Crystallography*, 50(5):1457–1477, Oct 2017.
- [37] J. L. Mañes. Existence of bulk chiral fermions and crystal symmetry. *Phys. Rev. B*, 85:155118, Apr 2012.
- [38] Vladimir Damljanić, Igor Popov, and Radoš Gajić. Fortune teller fermions in two-dimensional materials. *Nanoscale*, 9:19337–19345, 2017.
- [39] V Damljanić, N Lazić, A Šolajić, J Pešić, B Nikolić, and M Damnjanić. Peculiar symmetry-protected electronic dispersions in two-dimensional materials. *Journal of Physics: Condensed Matter*, 32(48):485501, sep 2020.
- [40] Marek Kopciuszynski, Mariusz Krawiec, Lucyna Żurawek, and Ryszard Zdyb. Experimental evidence of a new class of massless fermions. *Nanoscale Horiz.*, 5:679–682, 2020.
- [41] N Lazić, V Damljanić, and M Damnjanić. Fully linear band crossings at high symmetry points in layers: classification and role of spin–orbit coupling and time reversal. *Journal of Physics A: Mathematical and Theoretical*, 55(32):325202, aug 2022.
- [42] V Kopsky and D. B. Litvin. *International Tables of Crystallography Volume E: Subperiodic Groups*. Kluwer Academic Publishers, 2002.
- [43] T Hahn. *International Tables of Crystallography Volume A: Space-Group Symmetry*. Springer, 2005.
- [44] Koichi Momma and Fujio Izumi. *VESTA3* for three-dimensional visualization of crystal, volumetric and morphology data. *Journal of Applied Crystallography*, 44(6):1272–1276, Dec 2011.
- [45] Andy Knoll and Carsten Timm. Classification of Weyl points and nodal lines based on magnetic point groups for spin- $\frac{1}{2}$ quasiparticles. *Phys. Rev. B*, 105:115109, Mar 2022.
- [46] Ying-Ming Xie, Xue-Jian Gao, Xiao Yan Xu, Cheng-Ping Zhang, Jin-Xin Hu, Jason Z. Gao, and K. T. Law. Kramers nodal line metals. *Nature Communications*, 12:3064, May 2021.
- [47] Guang Bian, Tay-Rong Chang, Raman Sankar, Su-Yang Xu, Hao Zheng, Titus Neupert, Ching-Kai Chiu, Shin-Ming Huang, Guoqing Chang, Ilya Belopolski, Daniel S. Sanchez, Madhab Neupane, Nasser Alidoust, Chang Liu, BaoKai Wang, Chi-Cheng Lee, Horng-Tay Jeng, Chenglong Zhang, Zhujun Yuan, Shuang Jia, Arun Bansil, Fangcheng Chou, Hsin Lin, and M. Zahid Hasan. Topological nodal-line fermions in spin-orbit metal PbTaSe₂. *Nature Communications*, 7:10556, Feb 2016.
- [48] Zeying Zhang, Weikang Wu, Gui-Bin Liu, Zhi-Ming Yu, Shengyuan A. Yang, and Yugui Yao. Encyclopedia of emergent particles in 528 magnetic layer groups and 394 magnetic rod groups. *Phys. Rev. B*, 107:075405, Feb 2023.
- [49] Shao-Gang Xu, Baobing Zheng, Hu Xu, and Xiao-Bao Yang. Ideal nodal line semimetal in a two-dimensional boron bilayer. *The Journal of Physical Chemistry C*, 123(8):4977–4983, 2019.
- [50] V Damljanić and R Gajić. Existence of semi – Dirac cones and symmetry of two-dimensional materials. *Journal of Physics: Condensed Matter*, 29(18):185503, mar 2017.
- [51] V Damljanić. An example of diperiodic crystal structure with semi – Dirac electronic dispersion. *Optical and Quantum Electronics*, 50(7):272, jun 2018.